Оптический журнал

Расчет, проектирование и производство оптических систем

УДК 535, 617.7, 628.9

# Разработка крупноапертурного длиннофокусного объектива с изменением фокусного расстояния путем дискретного переключения линзовой компоненты

© 2021 г. Z. Zhang, W. Zheng, D. Gong, H. Li

**Представлена схема дискретного переключения линзовой компоненты зеркально-линзового крупноапертурного длиннофокусного объектива с широким полем зрения. Предлагаемая оптическая система включает телескоп по схеме Ньютона, содержащий коллиматорную и линзовую группы с переключаемым фокусным расстоянием. Высокое качество изображения как в длиннофокусном, так и в короткофокусном режимах при изменении условий работы и температуры обеспечивается перемещением коллиматорной группы. Значения функции передачи модуляции превосходят 0,5 на частоте Найквиста, 80% энергии концентрируется в кружке диаметром 0,025 мм (менее, чем два пиксела), в поле зрения максимальная дисторсия составляет 0,962% как в длиннофокусном, так и в короткофокусном режимах. Представленная система с переключаемым фокусным расстоянием обеспечивает высокое качество изображения при всех значениях фокусного расстояния, проста по конструкции и устойчива в работе.**

***Ключевые слова:*** *оптическая конструкция, система переменного фокуса, оптоэлектронный телескоп*

# Design of a zoom telescope optical system with large aperture, long focal length, and wide field of view via a catadioptric switching solution

© 2021 Zhenduo Zhang*, PhD (Physics); Wenbo Zheng*, graduate student (Physics); Dun Gong**, PhD (Physics); Hongzhuang Li**, PhD (Physics)

*Navigation College, Dalian Maritime University, Dalian, China

**Changchun Institute of Optics, Fine Mechanics and Physics, Chinese Academy of Sciences, Changchun, China

E-mail: gongdun@sina.com

Поступила в редакцию 06.07.2020

DOI:10.17586/1023-5086-2021-88-01-22-31

**This study presents a catadioptric switching solution for a zoom telescope optical system to achieve a large aperture, long focal length, and wide field of view. The proposed optical system combines a Newton-type main system with a collimator group and a switching zoom group. Further, clear imaging of long and short focal lengths under different operating ranges and temperatures is realized using a moving collimator group. For the field of view at both long and short focal lengths, the modulation transfer function exceeds 0.5 at the Nyquist frequency, 80% of the energy**

**is concentrated in a diameter of 0.025 mm (*i.e.*, less than two pixels), and the maximal distortion is 0.962%. The presented switching-zoom system exhibits high imaging quality for each focal length as well as a simple structure and stable performance.**

***Keywords:*** *optical design, zoom system, optoelectronic telescope.*

***OCIS codes:*** *110.2970, 280.4788, 350.4600*

## 1. INTRODUCTION

With the rapid development of technology in the aviation and aerospace fields, high technical requirements have been recently established for optoelectronic telescope systems. The goals of such systems include the rapid discovery and accurate identification of the target as well as real-time tracking, measurement, and imaging, which are also prerequisites for the development of modern aviation and aerospace technologies [1–11]. The photoelectric telescope systems are based on an advanced detection technology that integrates the optical, electronic, computer, signal processing, and control techniques. It uses optical systems to receive electromagnetic wave signals from targets for image capturing, tracking, and analysis as well as target recognition and to output various factors, including the target spatial position, motion speed and trajectory, and size.

With respect to photoelectric-telescope optical systems (PTOSs), a large aperture is required to achieve a strong detection capability [12–15]; a long focal length is required to perform high-resolution imaging and accurate measurements [16–18]. In addition, the detection field of view (FOV) should be sufficiently wide to achieve suitable detection efficiency [19–22]. However, the detection accuracy and FOV are contradictory optical parameters that cannot be simultaneously met by a PTOS with a fixed focal length. Therefore, the PTOS should adopt the zoom design method. There are two forms of zoom optical systems, *i.e.*, continuous zoom and switching zoom [23–28]. In a continuous-zoom system, the imaging quality varies considerably. Furthermore, the imaging quality is usually poor, and high measurement accuracy cannot be achieved in case of a wide FOV and long focal length (LFL). Further, the manufacture of a high-precision zoom cam is very difficult, and the zoom system is complex. On the other hand, the switching time of the switching zoom system constantly decreases because of the mechanical and electrical technological advances, allowing the tracking of fast-flying targets. In addition, when compared with continuous-zoom systems, switching-zoom systems have the following obvious advantages: simple structure and stable performance, independent design, testing, and assembly, high image quality and measurement accuracy at each focal length, and reduced hardware costs and short development cycle.

In this study, we designed a catadioptric switching-zoom optical system based on the requirements of an actual PTOS. The main technical specifications of the PTOS are presented in Section 2. The optical system design process, analytical methods, design results, and image-quality evaluation are presented in Section 3. Section 4 analyzes the focusing distances for different operating ranges and temperatures, and Section 5 generalizes the characteristics of the designed PTOS and denotes that the design results are in accordance with the requirements of the technical specifications.

## 2. TECHNICAL SPECIFICATIONS

The selected working band is 550–850 nm. According to the requirements of the PTOS, the diagonal FOV must exceed 1.7° in the search-and-discovery operation mode and the FOV of a single pixel should be higher than 0.65″ in a high-resolution-imaging and accurate-measurement operation mode. We use an array detector with a single pixel size of 12.5 μm and approximately 60-mm diagonal length.

In the search-and-discovery operation mode, the focal length of the optical system ($f_1'$) can be calculated as [29]

$$f_1' = \frac{l}{2\tan\left(\frac{\omega_1}{2}\right)} = \frac{A_d n}{2\tan\left(\frac{\omega_1}{2}\right)}, \qquad (1)$$

where, $l$ denotes the diagonal length of the detector, $\omega_1$ denotes the diagonal FOV of the optical system, $A_d$ denotes the pixel size, and $n$ denotes the number of diagonal pixels. The focal length $f'_1$ has been calculated to be 2020 mm when FOV = 1.7°. To ensure that the FOV is greater than 1.7°, by considering possible errors caused by the refractive index, processing, and adjustment of optical glass materials, $f'_1$ is slightly less than 2020 mm and is set as 2000 mm, Therefore, in this working mode, the full FOV of the optical system is 1.72°.

In the high-resolution-imaging and accuracy measurement operation mode, the focal length of the optical system ($f'_2$) can be obtained as

$$f'_2 = \frac{A_d}{2\tan\left(\frac{\omega_2}{2}\right)}, \quad (2)$$

where, $\omega_2$ denotes the FOV of a single pixel. The focal length $f'_2$ has been calculated to be 3800 mm when $\omega_2 = 0.65''$. However, we consider 4000 mm as the focal length of the optical system to allow a margin for imaging resolution. In this case, the FOV of a single pixel is approximately 0.62″ and the FOV is 0.86°.

According to the Rayleigh criterion, the diffraction spot diameter of the optical imaging system (φ) can be expressed as

$$\varphi = 2.44\lambda\frac{f'}{D} = 2.44\lambda F^{\#}. \quad (3)$$

Further,

$$F^{\#} = \frac{\varphi}{2.44\lambda}, \quad (4)$$

where, λ is the reference wavelength of 0.7 μm, $f'$ is the focal length of the optical system, $D$ and $F^{\#}$ are the diameter of the aperture stop and the $F$ number (*i.e.*, the inverse of the relative aperture) respectively. Further, the imaging diffraction spot diameter φ must be less than the outer circle diameter of the photodetector pixel (for strict control, usually less than the size of two pixels); therefore, $F^{\#}$ should be less than or equal to 10.3. Based on the system detection ability, design difficulty, and manufacturing cost, the $D$ value is 400 mm and $F^{\#} = 10$ in the case of a LFL, whereas the $D$ value 300 mm and $F^{\#} = 6.67$ in the case of a short focal length (SFL).

To satisfy the requirements of high-resolution imaging and accuracy of measurement, the modulation transfer function (MTF) of the PTOS should be greater than 0.25 at the Nyquist frequency [30]. The MTF can be calculated as follows [31, 32]:

$$\mathrm{MTF} = \mathrm{MTF}_{\mathrm{design}}\mathrm{MTF}_{\mathrm{man}}\mathrm{MTF}_{\mathrm{el}}\mathrm{MTF}_{\mathrm{geom}}. \quad (5)$$

Further,

$$\mathrm{MTF}_{\mathrm{design}} = \\ = \mathrm{MTF}_{\mathrm{static}}/(\mathrm{MTF}_{\mathrm{man}}\mathrm{MTF}_{\mathrm{el}}\mathrm{MTF}_{\mathrm{geom}}), \quad (6)$$

where, $\mathrm{MTF}_{\mathrm{design}}$ represents the MTF of the optical system design, $\mathrm{MTF}_{\mathrm{man}}$ represents the MTF of optical system manufacturing ($\mathrm{MTF}_{\mathrm{man}} = 0.85$) based on engineering experience [33], $\mathrm{MTF}_{\mathrm{el}}$ represents the MTF of the detector electronic system ($\mathrm{MTF}_{\mathrm{el}} = 0.93$) [34], $\mathrm{MTF}_{\mathrm{geom}}$ represents the MTF of the photodetector at the Nyquist frequency (approximately 40 lp/mm) ($\mathrm{MTF}_{\mathrm{geom}} = 0.637$) [30]. The $\mathrm{MTF}_{\mathrm{design}}$ of the optical system should be greater than 0.5 at the Nyquist frequency after calculation. In addition, the relative distortion of the optical system should be less than ±1% to ensure accurate measurement of the target trajectory. Table 1 summarizes the main technical specifications of the PTOS.

**Table 1. Main technical specifications of the PTOS**

| Specifications | Values | |
|---|---|---|
| | Search and discovery | Imaging and measurement |
| Spectral range, nm | 550–850 | 550–850 |
| Detector pixel size, μm | 12.5 | |
| Aperture, mm | 400 | 300 |
| Focal length, mm | 4000 | 2000 |
| FOV, deg | 0.86 | 1.72 |
| $\mathrm{MTF}_{\mathrm{design}}$ | ≥ 0.5 (Nyquist frequency) | |
| Relative distortion | < ±1% | |

## 3. OPTICAL SYSTEM DESIGN

### 3.1. Optical system layout

The proposed PTOS has a large optical aperture, wide spectrum, and LFL. The main system adopts the reflection type without chromatic aberration, which reduces the pressure on the

back-end refraction system to correct the chromatic aberration and secondary spectrum. The adoption of a Cassegrain-type system as the main system would result in a short optical-tube length. However, the main system comprises two aspherical mirrors, *i.e.*, main paraboloid and secondary hyperboloid mirrors, which are aspherical mirrors that are difficult and expensive to manufacture. Furthermore, the collimator lens group and switching zoom group should be located at the rear side of the main mirror. Therefore, the system cannot adopt a folded structure, which would result in a considerably large system volume.

Although the tube length of the Newton-type main system is greater than that of a Cassegrain-type system, the large-aperture primary mirror is spherical; therefore, it is cheap and easy to manufacture. In addition, its folding structure can be used as the overall layout, effectively reducing the system volume. Therefore, we adopted a Newton-type structure and used an existing spherical mirror with 400-mm diameter and 4000-mm radius as the primary mirror, which has a small relative aperture and low manufacturing cost.

The values of both the relative aperture and the FOV are small with respect to the LFL; therefore, it is mainly necessary to consider the secondary-spectrum correction. For an SFL with a large relative aperture and moderate FOV, it is necessary to consider corrections for both spherical and off-axis aberrations. To correct the spherical aberration of the primary mirror and the secondary spectrum of the zoom mirror group, a group of negative lenses is added in front of the first image. The switching zoom group must be placed in a parallel optical path to obtain high image quality for both LFL and SFL as well as a quick and stable mechanical-switching structure. A collimator lens is placed after the first image surface of the Newton-type main system to produce a parallel optical path. The optical system layout is presented in Fig. 1.

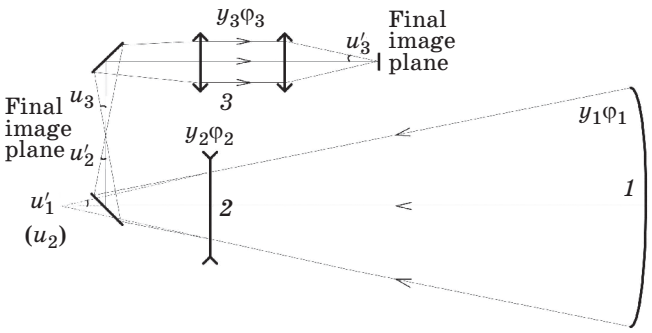


**Fig. 1.** The optical system layout. *1* — primary mirror, *2* — negative lens group, *3* — collimator and zoom lens group.

### 3.2 Calculation of the initial optical structure

The system comprises a primary mirror with optical power $\varphi_1$, a negative lens group with optical power $\varphi_2$, and collimator and zoom lens groups with optical power $\varphi_3$. The incident height of the marginal ray on the primary mirror, negative lens group, collimator, and zoom lens groups are $y_1$, $y_2$, and $y_3$ respectively. $u'_1$ represents the image aperture angle of the primary mirror, $u'_2$ represents the aperture angle before the first image plane, $u_3$ represents the aperture angle after the first image plane and is the opposite of $u'_2$, $u'_3$ represents the aperture angle before the final image plane. The initial structural calculation is mainly based on the LFL, because the optical system should exhibit a higher imaging quality at LFL than at SFL. For the SFL, only the zoom lens groups need to be replaced and optimized.

For the LFL, $D = 400$ mm, the primary mirror radius $R = 4000$ mm, the focal length of the primary mirror is $f'_P = R/2 = 2000$ mm, and $u'_1$ can be calculated as follows:

$$u'_1 = \frac{y_1}{f'_P} = \frac{D/2}{R/2} = 0.1. \tag{7}$$

To ensure that the system obstruction ratio is less than 0.2, consider the $y_2$ value to be 34 mm. The distance between the primary mirror and the negative lens group can be calculated as follows:

$$d_1 = f'_P - \frac{y_2 f'_P}{y_1} = 1660. \tag{8}$$

The negative secondary spectrum produced by the collimator and zoom groups are cancelled by the positive secondary spectrum produced by the negative lens group, and the achromatic effect can be achieved; therefore,

$$y_3{}^2\varphi_3 + y_2{}^2\varphi_2 = 0. \tag{9}$$

For the first image plane, assume that the focal length of the front system is $f'_F$. Then,

$$u'_2 = \frac{y_1}{f'_F} = \frac{200}{f'_F}. \tag{10}$$

The relation between the optical power and the aperture angle can be given as follows:

$$y_3\varphi_3 = u'_3 - u_3 = u'_3 - (-u'_2) = u'_3 + u'_2, \quad (11)$$

$$y_2\varphi_2 = u'_2 - u_2 = u'_2 - u'_1. \quad (12)$$

If the value of $y_3$ is large, it is easy to correct the residual spherical aberration, but it will increase the size of the whole optical system and is limited by the given space. If the value of $y_3$ is small, it will increase not only the difficulty of lens processing but also the difficulty of structural arrangement because the distance between the first image plane and the collimator lens group will be short. The $y_3$ value is selected as 12 mm by considering the difficulty of aberration correction, system space, system structure, and lens-processing difficulty. $u'_3 = y_1/f'_L = 200/4000 = 0.05$. By combining Eqs. (9)–(12), $f'_F$ is calculated to be 3286 mm, and the focal length of the negative lens group ($f'_N$) can be calculated as follows:

$$f'_N = \frac{1}{\varphi_2} = -869 \text{ mm}. \quad (13)$$

The distance between the negative lens group and the first image plane ($d_2$) can be calculated as follows:

$$d_2 = \frac{f'_F y_2}{y_1} = 559 \text{ mm}. \quad (14)$$

The distance between the first image plane and the collimator and zoom lens groups ($d_3$) can be calculated as follows:

$$d_3 = \frac{d_2 y_3}{y_2} = 197 \text{ mm}. \quad (15)$$

The focal length of the collimator lens group ($f'_C$) is equal to $d_3$ ($f'_C = 197$ mm). The magnification of the collimator and zoom lens groups for the LFL ($M_L$) and SFL ($M_S$) can be calculated as follows:

$$M_L = \frac{f'_{DL}}{f'_F} = \frac{4000}{3286} = 1.22, \quad (16)$$

$$M_S = \frac{f'_{DS}}{f'_F} = \frac{2000}{3286} = 0.61, \quad (17)$$

where, $f'_{DL}$ and $f'_{DS}$ are the system focal lengths at LFL and SFL respectively. The focal lengths of the zoom lens group for the LFL ($f'_{ZL}$) and the SFL ($f'_{ZS}$) can be calculated as follows:

$$f'_{ZL} = f'_C M_L = 240 \text{ mm}, \quad (18)$$

$$f'_{ZS} = f'_C M_S = 120 \text{ mm}. \quad (19)$$

### 3.3. Optimal design considerations

The collimator lens group should be able to adjust the focal length and maintain a stable image plan in addition to the collimating beam; therefore, its structure cannot be considerably complex. The combination of a single lens and double lens can perform the aforementioned functions very well; however, a certain residual aberration that should be corrected by the zoom lens group still remains.

The zoom lens groups must have sufficient rear working distance for the convenience of switching between LFL and SFL and to reserve space for the filter between the final lens and detector. For the design of zoom lens groups, in the case of SFL, the object FOV of the optical system is wide, and the corresponding image FOV is further increased after the collimator group. Therefore, the SFL zoom group adopts the reverse telephoto structure, the FOV is compressed through the front-end negative elements, and the rear working distance is increased through the separation of negative and positive focal power to ensure that the position of the final image plane under the SFL and LFL is constant. In case of LFL, through the separation of positive and negative focal power and the complication of the zoom lens group of LFL to shorten the rear working distance, to ensure that the position of the final image plane is the same as that in the case of SFL. Due to the different beam apertures under the LFL and the SFL, it is necessary to place two stops with different apertures into the zoom-lens-group cylinder at the pupil position before the zoom lens groups to synchronously complete the stop change and the LFL and SFL switching.

The level of aberration correction in an optical system directly affects the image contrast and resolution and finally affects the operating range as well as the imaging and measurement accuracy. The Newton-type main optical system

cannot appropriately correct the off-axis aberrations, including coma and lateral chromatic aberration. The telescopic system comprising the main optical system and the collimator group does not have the ability to correct the off-axis aberrations. The system off-axis aberration can be corrected only by designing and optimizing the LFL and SFL zoom lens groups separately. The optical power must be properly distributed during aberration correction to prevent the zoom lens group from producing a secondary spectrum when using only ordinary optical glass. During this process, the positions of the long and short focal image planes must be strictly maintained constant, and the distortion of the optical system must be controlled.

### 3.4. Design result and image quality evaluation

We used the optical design software CODE V to optimize the optical system after determining the initial structural parameters, analyzing the characteristics of each component, and integrating the different lens group structures. For optimization, the Error Function type is selected to be the Transverse Ray Aberration and the constraint parameters include the effective focal length, overall length, and minimum air center thickness. The optical layouts of LFL and SFL are shown in Fig. 2.

By optimizing the optical system, the MTF values for each FOV in case of LFL and SFL are

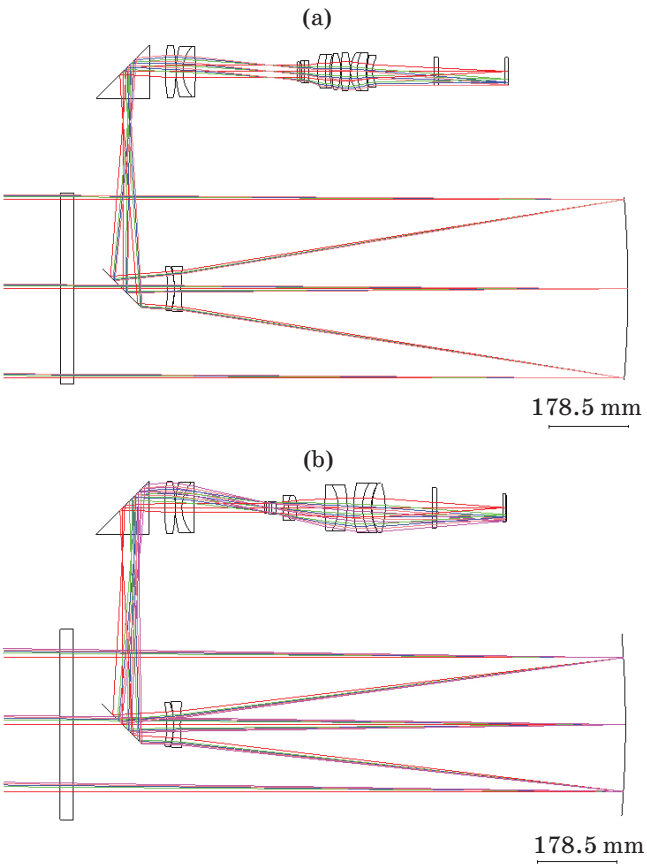


**Fig. 2.** The optical layout of (a) LFL and (b) SFL.

**Table 2. The MTF values for different FOVs in case of LFL and SFL at the Nyquist frequency**

| FOV, deg | | LFL, mm | SFL, mm |
|---|---|---|---|
| 0.0 | Tangential plane | | |
| | Sagittal plane | 0.560 | 0.583 |
| | Average value | | |
| 0.3 | Tangential plane | 0.563 | 0.578 |
| | Sagittal plane | 0.558 | 0.565 |
| | Average value | 0.561 | 0.572 |
| 0.5 | Tangential plane | 0.564 | 0.563 |
| | Sagittal plane | 0.554 | 0.564 |
| | Average value | 0.559 | 0.564 |
| 0.7 | Tangential plane | 0.560 | 0.546 |
| | Sagittal plane | 0.549 | 0.561 |
| | Average value | 0.555 | 0.554 |
| 1.0 | Tangential plane | 0.529 | 0.554 |
| | Sagittal plane | 0.527 | 0.518 |
| | Average value | 0.528 | 0.536 |

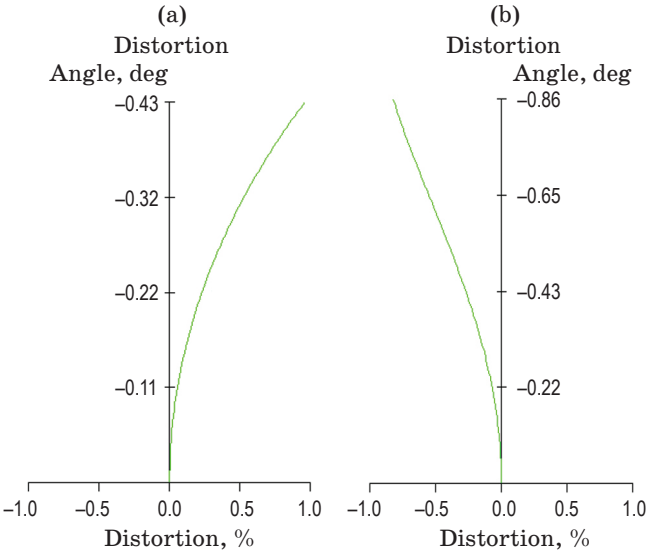


**Fig. 3.** Relative distortion curves for different fields of view in case of (a) LFL and (b) SFL.

**Table 3. The spot diameters corresponding to 80% of the power for different FOVs**

| FOV, deg | LFL, mm | SFL, mm |
|---|---|---|
| 0.0 | 0.022 | 0.019 |
| 0.3 | 0.022 | 0.019 |
| 0.5 | 0.022 | 0.020 |
| 0.7 | 0.022 | 0.020 |
| 1.0 | 0.024 | 0.021 |

**Table 4. The relative distortion values for different FOVs in case of LFL and SFL**

| FOV, deg | LFL, % | SFL, % |
|---|---|---|
| 0.3 | 0.082 | −0.101 |
| 0.5 | 0.230 | −0.270 |
| 0.7 | 0.457 | −0.491 |
| 1.0 | 0.962 | −0.822 |

higher than 0.5 at the Nyquist frequency, the image quality is good, and the image quality exhibits good consistency on the axis and off-axis. The values of each FOV at the Nyquist frequency are summarized in Table 2.

The spot diameters corresponding to 80% of the power for each FOV in case of LFL and SFL are presented in Table 3 and exhibit good consistency on the axis and off-axis. The spot diameter corresponding to 80% of the power of each FOV is within 0.024 mm, which is less than the size of two pixels.

The relative distortion curves for different FOVs in case of LFL and SFL are displayed in Fig. 3, and Table 4 reports the corresponding relative distortion values. The maximal distortion for all the FOVs is 0.962%, smaller than ±1%.

## 4. FOCUSING ANALYSIS OF THE OPTICAL SYSTEM

The system needs to adopt a suitable zooming process because of the variations in the target observation distance and temperature. This is realized by moving the collimator group. The position change of the final image plane owing to the different operating ranges is the same for LFL and SFL. However, the LFL and SFL systems have different zoom lens groups and are

**Table 5. Focusing distances for different operating ranges**

| Operating range, km | Focusing distance, mm |
|---|---|
| 1 | +6.25 |
| 3 | +2.08 |
| 5 | +1.25 |
| 7 | +0.89 |
| 9 | +0.69 |

**Table 6. Focusing distances for different temperatures**

| Temperature, deg | Focusing distance, mm | |
|---|---|---|
| | LFL | SFL |
| −35 | +1.31 | +1.67 |
| −20 | +0.95 | +1.18 |
| 0 | +0.48 | +0.56 |
| 20 | 0.00 | 0.00 |
| 30 | −0.21 | −0.34 |
| 40 | −0.44 | −0.64 |
| 55 | −0.77 | −1.08 |

affected differently by the temperature change; consequently, their focusing distances are not identical. Tables 5 and 6 summarize the focusing distances of the optical system corresponding to different operating ranges and temperatures respectively. The + and — signs indicate the focusing in the direction of the final image plane and the first image plane respectively.

## 5. DISCUSSION OF THE CATADIOPTRIC SWITCHING SOLUTION

According to the design results, we have completed the development and application of a PTOS based on a catadioptric switching solution, and the principal layout of the PTOS is shown in Fig. 4. The research team has experience with the design, testing, assembly, integration, and application of the system, and the main features and relevant engineering experience are summarized as follows:

1) With respect to the design of a continuous-zoom system, there are many moving optical elements; the design of this system is complex

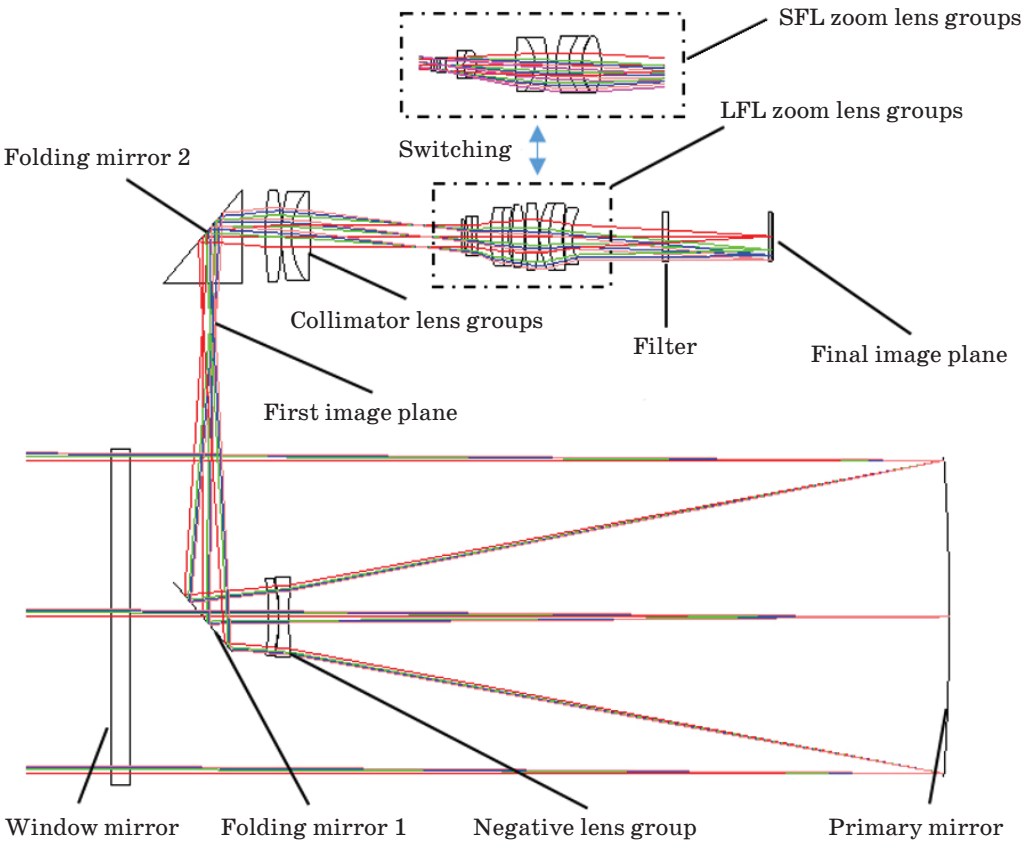


**Fig. 4.** The principal layout of the PTOS based on a catadioptric switching solution.

and difficult, and the imaging quality cannot become ideal at all focal-length positions. For the catadioptric switching system, there are few lenses and high transmissivity. Under the two focal lengths, each zoom lens group is designed separately and the imaging quality at the two focal lengths is significantly higher than that of a continuous-zoom system; therefore, it is easy to design and achieve the technical specifications.

2) With respect to testing and assembly, the primary mirror of the catadioptric switching system is a spherical mirror, and it is convenient to finish the primary mirror processing and the surface characterization testing on the supporting structure using a ZYGO interferometer. In the first image surface formed by the primary mirror and its negative lens group, the star point method is used to guide the assembly of the negative lens group, so that its axial FOV has an ideal imaging quality. A ZYGO interferometer is used to test and guide the adjustment of the collimator lens group to ensure that the collimating beam is close to the ideal. The centering method is used to adjust the LFL and SFL zoom lens groups respectively, and the adjustment effect is tested by the star point method. After the whole system is integrated, the collimator is used to test and adjust the final image plane consistency and optical axis deviation. The whole testing and assembly process can be easily realized. For a continuous-zoom system, the optical axes of the zoom group and the compensation group are inconsistent when they move during the zoom process, and the image plane is inconsistent under different focal lengths, which complicates testing and assembly.

3) With respect to integration, there are few moving elements in a catadioptric switching structure. However, there is no axial moving component in a continuous zoom, and there is no need for a cam; therefore, the mechanical structure is simple, the size is small, and the integration is convenient.

4) With respect to applications, when a photoelectric telescope system performs observations, it can quickly switch to the LFL to observe the detailed characteristics of the target after detecting the target at SFL. The switching

time from SFL to LFL is less than 1 s, which is significantly faster than the continuous-zoom solution, and it can adapt to the changing application and observation environment. The two zoom lens groups are integrated on the same load frame with circular motion, and the motor directly drives the load frame to complete the switching in the optical path. The positioning accuracy is high, the performance is stable, and the cost is low. Thus, the catadioptric switching solution can simultaneously obtain a large aperture, large FOV, and long focal distance, which not only ensures the search efficiency of the photoelectric telescope system but also realizes high-accuracy imaging of a long-operating-range target.

## 6. CONCLUSION

A PTOS should exhibit a large aperture, LFL, and wide FOV to attain high detection ability, resolution, accuracy, and efficiency. However, the LFL and large FOV are contradictory optical parameters and cannot be simultaneously achieved using the conventional optical design method; therefore, this study proposed a catadioptric switching solution. The proposed optical system comprises a primary mirror, a negative lens group, and collimator and zoom lens groups when considering the structure size and aberration correction for both LFL and SFL. Only ordinary optical glass is used to correct the secondary spectrum via optical-power distribution. The optical system can be focused by moving the collimator lens group. Further, the focusing distances are calculated for different operating ranges and temperatures. During the focusing process, the final image-plane position of the optical system remains constant, and good imaging quality can be obtained. The MTF values for each FOV in case of LFL and SFL exceed 0.5 at the Nyquist frequency. The spot diameter corresponding to 80% of the power of each FOV is within 0.025 mm, which is less than the size of the two pixels; the maximal distortion of all FOV is 0.962%, which is smaller than ±1%. The imaging qualities with respect to the LFL and SFL of the optical system are good and satisfy the technical specification requirements. Thus, a photoelectric telescope optical system with a large aperture, LFL, and wide FOV can be realized. Furthermore, we will study the zoom optical design method of the large-aperture photoelectric telescope, consider the impact of atmospheric turbulence and stray light on the imaging quality, and study the speckle image restoration technology detect and image darker and farther targets.

This research was supported by Fundamental Research Funds for the Central Universities (3132020130).

### *REFERENCES*

1. *Werth M., Gerwe D., Griffin S., Calef B., Idell P.* A ground-based optical imaging of GEO satellites with a rotating structure in a sparse aperture array // Proc. IEEE Aerospace Conf. 2–9 March 2019. Big Sky, MT, USA. P. 1–11.
2. *Chang S.-T., Lin Y.-C., Lien C.-C., Huang T.-M., Tsay H.-L., Miau J.-J.* The design and assembly of a long-focal-length telescope with aluminum mirrors // Proc. Int. Conf. Space Optics. 9–12 October 2018. Chania, Greece. P. 245.
3. *Ramsay M., Sobek R., Canzian B., Maloney J.* Future ground-based telescopes design requirements // Proc. SPIE Int. Soc. Opt. Eng. 2010. V. 7733. Paper 77330Y.
4. *Lo Presti D., Gallo G., Bonanno D.L., et al.* The MEV project: Design and testing of a new high-resolution telescope for Muography of Etna Volcano // Nuclear Instrum. Meth. Phys. Res. 2018. V. 904. P. 195–201.
5. *Erbas B., Underwood C.I.* Active focusing system for an earth imaging reflecting telescope // Proc. Conf. RAST. 9–11 June 2005. Istanbul, Turkey. P. 545–550.
6. *Israni D., Patel S., Shah A.* Comparison of different techniques of camera autofocusing // Proc. Int. Conf. Info. Commun. Technol. Intell. Sys. 1. 28–29 November, 2015. Ahmedabad, India. P. 125–135.
7. *Etherton J., Rees P.C.T., Steele I.A.* Telescope design and efficiency // Proc. Observ. Opera. Optimize Sci. Return II: Astro. Tele. Instru. 25 July 2000. Munich, Germany. P. 298–313.
8. *Steve H., Elliott H.* High-resolution speckle imaging // Phys. Today. 2018. V. 71. P. 78–79.
9. *Hope D.A., Jefferies S.M., Hart M., Nagy J.G.* High-resolution speckle imaging through strong atmospheric turbulence // Opt. Exp. 2016. V. 24. № 11. P. 12116.

10. *Wang R.-Q., Zhang Z.-Y., Guo C.-L., Xue D.-L., Liu H.* Design/fabrication and performance test of a diffractive telescope system with high diffraction efficiency // Acta Photon. Sin. 2017. V. 46. № 3. P. 46.
11. *Cassaing F., Mugnier L.M.* Optimal sparse apertures for phased-array imaging // Opt. Lett. 2018. V. 43. № 19. P. 4655–4658.
12. *Sanders G.H.* The thirty meter telescope (TMT): An international observatory // J. Astrophys. Astr. 2013. V. 34. P. 81–86.
13. *Stepp L.M., Gilmozzi R., Hall H.J., Gunnels S.* The Giant Magellan telescope (GMT): Gregorian instrument rotator bearing // Proc. SPIE Int. Soc. Opt. Eng. 2014. V. 9145. Paper 91455E.
14. *Huang Z., Huang R., Xue X.* Analysis of SNR for high-orbit target detected by ground-based photoelectric system // Appl. Sci. 2018. V. 8. № 12. P. 2604.
15. *Bourgois R., Geyl R.* Manufacturing ELT optics: Year 2 report // Optical Fabrication and Testing. 2019. Paper OM3A.3.
16. *Metwally M., Bazan T.M., Eltohamy F., Mahmoud F.* Optical design, tolerance analysis, and baffling of very high-resolution satellite telescopes // Proc. Int. Conf. Electri. Eng. 25 March 2018. Chengdu, China. P. 1–11.
17. *Massie N.A., Oster Y., Poe G., Seppala L., Mike S.* Low-cost, high-resolution telescopes for imaging low-Earth orbit satellites // Proc. SPIE Int. Soc. Opt. Eng. 1990. V. 1117. P. 313–329.
18. *Massie N.A., Oster Y., Poe G., Seppala L., Mike S.* Low-cost, high-resolution, single-structure array telescopes for imaging of low-Earth-orbit satellites // Appl. Opt. 1992. V. 31. № 4. P. 447–456.
19. *Sun R.Y., Yu S.X.* Precise measurement of the light curves for space debris with wide field of view telescope // Astrophy. Space Sci. 2019. V. 364. № 3. Paper 39.
20. *Hui J., Ma H.-T., Yan C.-X., Zheng Y.Q., Jiang H.-l., Lin, J.* Wide spectrum, a large field of view telescope system design small distortion // Proc. SPIE Int. Soc. Opt. Eng. 2013. V. 8759. Paper 87590X.
21. *Park H.S., Axelrod T.S., Colella N.J., Colvin M.E., Ledebuhr A.G.* Realtime tracking system for the wide-field-of-view telescope project // Proc. SPIE Int. Soc. Opt. Eng. 1989. V. 1111.
22. *He C.L., Wei H.G., Shen M.Z.* Numerical analysis of anisoplanatism of wide-field-of-view telescope imaging through turbulent atmosphere // Opto-Electronic Eng. 2011. V. 38. № 12. P. 13–17.
23. *Guo X.H., Lu T.L., Zhang W., Wang F.P., Zhao J.* Design of a continuously zoom optical system // Proc. Int. Conf. Opt. Instrum. Technol. 28–30 October 2017. Beijing, China. P. 66.
24. *Tian T.-Y., Wang H.* Optical zoom system with long focal length and large aperture // Opt. Prec. Eng. 2014. V. 22. № 9. P. 2369–2374.
25. *Li Z., Dai M., Li J.-Q.* Continuous zooming imaging system driven by stepping motors // Chinese Opt. 2018. V. 11. № 10. P. 779–789.
26. *Yan P.P., Liu K., Duan J., Jiang K., Shan Q.S.* Switch-zoom optical system design of large aperture ground-based photoelectric detection // Proc. SPIE Int. Soc. Opt. Eng. 2016. V. 9682. Paper 968215.
27. *Miao W.J., Luo X.S., Lu J., Li Z.W., Du B.Q., Ji R.* Five switched zoom optical system for focometer // Opt. Techni. 2018. V. 44. № 2. P. 177–182.
28. *Yang L.-H., Li J., Tao Y., Lin J., Meng J.-H.* Confocal design for switch-zoom optical system // J. Appl. Opt. 2014. V. 35. № 3. P. 386–390.
29. *Li Z.* Research on simulation technology of photoelectric theodolite infrared imaging in complex environment // Thesis. Master., Xidian University, Dept. of Pys. an Electr. Eng. 2014. P. 109. (Citable URI: https://kns.cnki.net/kcms/detail/detail.aspx?FileName=1017300147.nh&DbName=CMFD2018)
30. *Han C.-Y., Wang H.* Performance optimization of electro-optical imaging systems // Opt. Prec. Eng. 2015. V. 23. № 1. P. 1–9.
31. *Zhang Y.* Applied optics. 4th ed. Beijing: Publishing House of Electronics Industry, 2015. 620 p.
32. *Wang Z.* The Manual of optical technology. Beijing: Publishing House of Mechanical Industry, 1987. 1762 p.
33. *Han C.* MTF analysis and radiation calibration of space camera. Beijing: Science Publishing Company, 2005. 564 p.
34. *Boreman G.D.* Modulation transfer function in optical and electro-optical systems // Russ. Chem. Rev. 2001. V. 71. № 2. P. 159–179.